Thermodynamic simulation for the investigation of marine Diesel engines

CrossMark

A.J. Murphy *, A.J. Norman, K. Pazouki, D.G. Trodden

Newcastle University, Newcastle upon Tyne, United Kingdom

ABSTRACT

Emissions in the shipping industry are a major environmental concern and IMO regulations are increasingly stringent. Existing methods to assess marine exhaust gas emissions require large and specialised input data-sets. There is therefore a requirement for a methodology which can resolve the dilemma of estimating time-varying gas properties with sufficient accuracy to, for example, predict NO_X emissions, whilst also being applicable across the variety of engine types and operational modes that prevail in the marine context, for which there is often sparse input data.

In this paper, the influence upon thermal efficiency and the prediction of gas temperature time-histories of differing levels of sophistication in modelled gas properties and composition models is therefore evaluated, as is the effect of modelling engine losses. Using the results of this study, a coupled dynamic-thermodynamic engine simulation in the time-domain is developed, capable of modelling engine performance across the full range of operational conditions (speed and load), including part-load and transient conditions. The simulation is validated against the Otto cycle and through simulations of experimental engine data, the model is shown to successfully predict actual engine performance across a range of engine load conditions.

1. Introduction

1.1. Exhaust gas emissions in the marine industry

The IMO estimated that in 2007 maritime traffic produced 870 million tonnes of CO_2, representing 2.7% of global total, and 36.3 million tonnes of other environmentally harmful combustion products including NO_X, SO_X, PM and CO (Buhaug et al., 2009). These emissions are of major concern because of their contribution to anthropogenic climate change and their effects on environmental and human health. This is also reflected in the recent proliferation of regulations and research efforts for reducing exhaust gas emissions from ships.

While CO_2 emissions, an inevitable combustion product of carbon-based fuels, are projected to increase with the forecasted growth in international shipping (UNCTAD, 2013), they can be reduced by reducing fuel consumption through more efficient engine design and operation. Other air pollutants such as NO_X, PM and CO, can be reduced independently of fuel consumption. For example, the temperature of the cylinder gasses, oxygen abundance and residence time are the main factors affecting the formation of NO_X, the bulk of which is formed by post flame reactions (Write, 2000), whereas, CO emissions are primarily controlled by the fuel/air equivalence ratio (Heywood, 1988).

Because these emissions are highly dependent on not only engine design but also on engine operation, it makes their effective control potentially achievable but their estimation particularly difficult. This is a specific challenge in the maritime industry because there is a wide variety of; engine types, engine size, engine age, marine fuel types, etc. Furthermore, there are usually multiple engines on board individual ships, often with relatively sparse technical data available to the analyst. These are being operated in part- and transient-load conditions especially in ports, where the production of poisonous air pollutants is in the vicinity of high population density, where they cause the most harm. To compound the situation further, the use of steady-state emission data to estimate engine emissions in transient operation can cause errors by up to a factor of two (Lloyd's Register of Shipping, 1995).

1.2. Engine simulation in the marine industry

A number of thermodynamic models of marine Diesel engines have been developed for various applications including; the detection of faults (Hountalas, 2000), the training of Navy engine crews (Chesse et al., 2004) and as an aid to engine design (Heywood, 1988). Hountalas (2000) claims that, due to the uniqueness of

Nomenclature

A (m^2)   net piston face area perpendicular to the direction of piston travel

C_v (J kg^{-1} K^{-1}) specific heat capacity at constant volume (isochoric)

C_P (J kg^{-1} K^{-1}) specific heat capacity at constant pressure (isobaric)

F_C (N)   force acting through the connecting rod

F_P (N)   net force acting on piston face due to gas pressure

g (m s^{-2}) acceleration due to gravity

H_d (m)   perpendicular distance between connecting rod and shaft centre of rotation

J_s (kg m^2) total shaft mass moment of inertia

m (kg)   mass

m_p (kg) Piston mass

P (Pa)   absolute gas pressure

$q, \dot{q}$ (J kg^{-1}, W kg^{-1}) specific heat, rate of specific heat with subscripts as appropriate

R (J kg^{-1} K^{-1}) specific gas constant

T_n (K)   temperature with or without relevant cycle point, n, as appropriate

T_p (N m) total externally applied torque acting on the shaft

$u, \dot{u}$ (J kg^{-1}, W kg^{-1}) specific internal energy, rate of change of specific internal energy

v_n (m^3 kg^{-1}) specific volume with or without relevant cycle point, n, as appropriate

$w, \dot{w}$ (J kg^{-1}, W kg^{-1}) specific work, rate of specific work with subscripts as appropriate

$x, \dot{x}, \ddot{x}$ (m, m s^{-1}, m s^{-2}) linear (piston) position, velocity, acceleration

γ (dimensionless) ratio of constant pressure to constant volume specific heat capacities

ΔP (Pa) difference between internal cylinder pressure and external gas pressure

$\theta, \dot{\theta}, \ddot{\theta}$ (rad, rad s^{-1}, rad s^{-2}) angular (shaft) position, velocity, acceleration

ϕ (rad) connecting rod angle

---

marine Diesel engines and their operation, computer programmes for marine applications must be specifically designed, requiring that each application requires a different model.

Although complex and time consuming, CFD methods can be used to model a specific marine Diesel engine, taking into account the specifics of cylinder shapes and injection spray patterns (Kilpinen, 2010). The time, computing power and data requirement of these techniques are unattainable for some applications; consider, for example, the variation in operation and engine type for a complete harbour emissions model or an estimate for a shipping channel. Furthermore, due to their complexity, CFD methods are also very sensitive to inaccurate inputs and incorrect input processing, as noted by Kilpinen (2010) who presents one such model that was found to be over-predicting NO emissions by an order of magnitude.

1.3. Paradigm of NO$_X$ estimation

Whilst stoichiometric combustion equations can be used to predict exhaust species resulting from complete combustion such as CO$_2$ and SO$_2$ with reasonable accuracy, prediction of species resulting from incomplete combustion, e.g. CO, SO, HC, etc. and, of particular concern for marine engines, NO$_X$, is more challenging. The production of NO, for example, is highly dependent upon temperature variation and residence time. Amongst the Oxides of Nitrogen that are produced in engine combustion, NO is the most prevalent, however, this is almost completely converted into nitrogen dioxide (NO$_2$) when exposed to air under atmospheric conditions.

The formation of thermal NO can be modelled using the reaction method of Zeldovich (1946), expanded upon by Baulch et al. (1991). Following some simplifying arguments, Merker et al. (2005) derive Eq. (1), relating rate of concentration of NO production with temperature and concentrations of nitrogen and oxygen.

$$\frac{d[NO]}{dt} = 4.7 \times 10^{13} [N_2][O_2]^{1/2} \exp\left(-\frac{67837}{T}\right) \; [\text{k mol m}^{-3}\text{s}^{-1}] \quad (1)$$

The research motivation for the work reported in this paper is therefore to ameliorate modelling and simulation tools that address the challenge of providing an adequate compromise between the accuracy required to permit reasonable estimations of exhaust gas emissions from marine Diesel engines within the limits imposed by the challenges in this field as described in the final paragraph of Section 1.1 – specifically the wide variety of engine types, fuels, varying operational conditions, etc. in the marine industry.

Noting that the prediction of emissions of interest are principally governed by accurate predictions of temperature and pressure variations over the course of the Diesel engine cycle, as indicated in Eq. (1), under realistic operating conditions, including part- and transient-load operations this paper initially investigates the sensitivities of the underlying thermodynamic assumptions for Diesel engine models, specifically including effects of temperature variation on the gas properties. For simplicity, these investigations are undertaken using steady-state modelling approaches.

A first principles model is ultimately provided, necessarily taking a time-domain approach, with sufficient accuracy for modelling the performance of marine Diesel engines, while requiring only a modest level of engine-specific data. The developed model is named the Marine Engine System Simulation (MESS). Heat flow is modelled in two parts; one accounting for heat addition from fuel combustion and the other due to heat loss from the cylinder. Temperature-dependent and gas-composition-dependent properties of the cylinder gases, including or excluding residual exhaust gases, can be analysed over varying levels of sophistication and is suited to providing the necessary input data for solving, for example, Eq. (1).

2. Steady-state thermodynamic engine modelling

To evaluate the sensitivities of engine simulation results to the level of sophistication of the thermodynamic model, a steady-state approach was initially considered in order to demonstrate the improvement in accuracy by accounting for the temperature variation in gas properties and gas composition due to fuel combustion. The results of this investigation are applied to the more sophisticated simulations of Sections 3 and 4.

The air-standard *dual cycle*, as illustrated in Fig. 2.1, is the accepted steady-state idealisation of the marine Diesel engine cycle (e.g. Jackson et al., 2012) and, while it cannot accurately predict absolute values for engine outputs, e.g. it overestimates efficiency with values around 60–70% as compared to even the most efficient marine Diesel engines with typical maximum efficiencies up to 54% (Woodyard, 2009), it does provide a benchmark against which to compare more sophisticated cycle models, e.g. as presented in Section 4.

2.1. Varying gas properties and composition

For the *air-standard* dual cycle, invariant gas properties are assumed, typically $C_v = 718\,J/kg\,K$ and $C_P = 1005\,J/kg\,K$. These values are those for dry air at approximately 35 °C (e.g. Keenan et al., 1983). In fact, as illustrated in Fig. 2.2 and Table 2.1, specific heat capacities of gases are highly dependent on temperature and gas composition (Payri et al., 2011) and are substantially higher than the aforementioned standard values at temperatures typically encountered in a dual cycle analysis.

For the purposes of including the temperature-dependence of gas properties in a thermodynamic model, the approach adopted here is to use a linear or polynomial equation, based on the tabulated values in the *JANAF Thermochemical Tables* (Chase et al., 1986), so that the specific heat capacities of each gas, as a function of temperature, are in the form

$$C_v = a_0 + a_1 T + a_2 T^2 + \ldots + a_n T^n \tag{2}$$
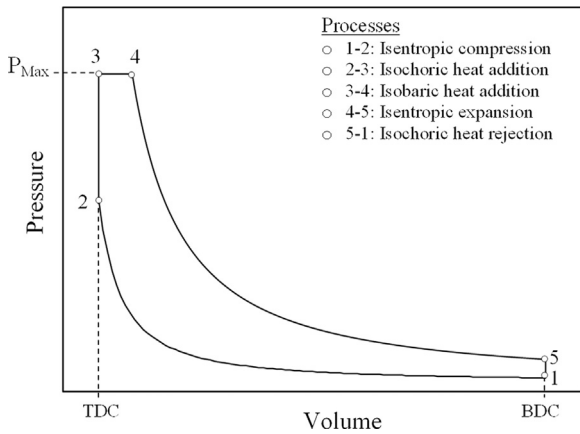

Fig. 2.1. Pressure–volume diagram of the air-standard dual cycle. Cycle points 1–5 are referred to in the analysis in Section 2.1.

and

$$C_P = b_0 + b_1 T + b_2 T^2 + \ldots + b_n T^n. \tag{3}$$

A further increase in the sophistication of the dual cycle model is to consider the effect that the variation in gas composition has on calculated results, analogous to presence of exhaust gas in the cylinder post combustion. For this analysis, the temperature-dependent exhaust gas properties are calculated and substituted in the place of the properties of dry air. For the dual cycle analysis the gas composition is assumed to change at the end of the compression process (after point 2, in Fig. 2.1). A yet more detailed approach, used for the time-based simulation of Section 3, accounts for the progressive change in cylinder gas composition through the combustion process.

The assumed exhaust gas properties are calculated for each dual cycle following a similar procedure to Ferguson (1986). That is, an assumed mass of fuel is calculated from (Eastop and McConkey, 1993)

$$Q_{in} = q_{in} m_a = m_f LCV. \tag{4}$$

and, from the fuel mass, m_f, the proportions of the species in the exhaust gas are estimated using an assumed fuel specification and complete combustion.

The temperature-dependent and composition-dependent gas properties at any given point in the cycle are then calculated by combining Eqs. (2) and (3) with Gibbs–Dalton law i.e.,

$$C_v = \frac{\sum (m_i C_{vi})}{m}, \tag{5}$$

and

$$C_p = \frac{\sum (m_i C_{pi})}{m}. \tag{6}$$

Table 2.1 provides the coefficients for the fifth-order polynomials for the principal gas species required in this analysis for use in Eqs. (2) and (3).

By integrating the temperature change over each cycle process, the analysis incorporates the temperature-dependent specific heat
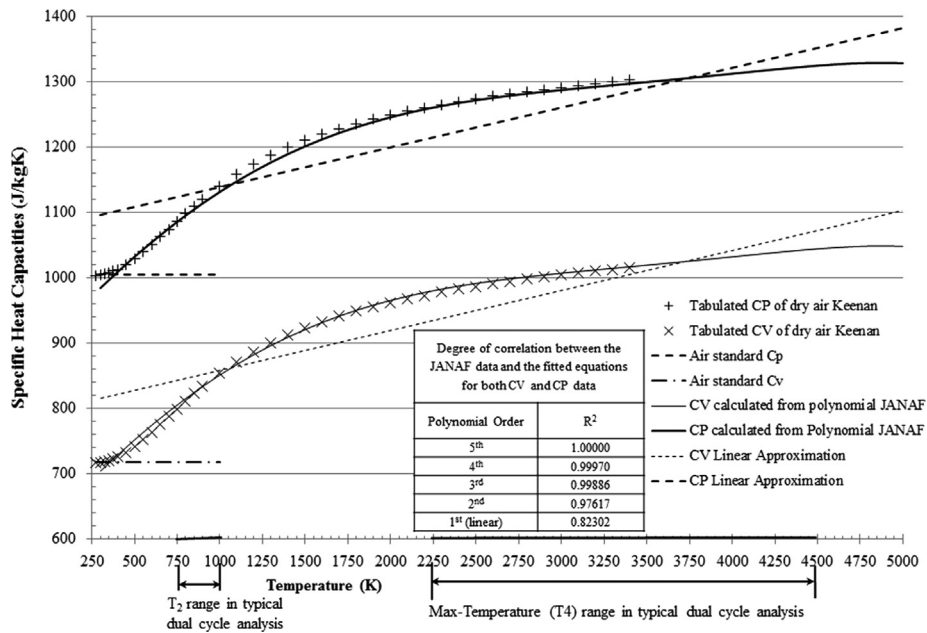

Fig. 2.2. Specific heat capacities of dry air compared as a fifth-order polynomial and a linear approximation in the range 300–5000 K from the JANAF Tables (Chase et al., 1986) and values tabulated in Keenan's gas tables in the range 300–3400 K (Keenan et al., 1983). Typical temperature ranges indicated are a guide to values often encountered in air-standard dual cycle calculations. Although not all curves are plotted, for guidance, the R^2 values for the different polynomial approximations of the JANAF data are presented in the inserted table.

Table 2.1
Coefficients for C_v and C_P of individual gasses as a fifth-order polynomial, calculated from data in the range 300–5000 K (Chase et al., 1986). The coefficients for C_v and C_P of dry air are calculated using the Gibbs–Dalton Law and the proportion of dry air by mass from (Eastop and McConkey, 1993).

C_v	a_0	a_1	a_2	a_3	a_4	a_5	Proportion of dry air by mass (%)
N_2	6.6508218510^2	$1.95531858 \times 10^{-1}$	$5.28590534 \times 10^{-5}$	$-5.87732131 \times 10^{-8}$	$1.42753440 \times 10^{-11}$	$-1.11597603 \times 10^{-15}$	75.53
O_2	5.08726781×10^2	$5.68661040 \times 10^{-1}$	$-3.53970739 \times 10^{-4}$	$1.22148573 \times 10^{-7}$	$-2.05538458 \times 10^{-11}$	$1.32813770 \times 10^{-15}$	23.14
Ar	3.11550000×10^2	0.00000000×10^0	0.00000000×10^0	0.00000000×10^0	0.00000000×10^0	0.00000000×10^0	1.28
CO_2	3.45780031×10^2	1.30016198×10^0	$-8.29823310 \times 10^{-4}$	$2.70087323 \times 10^{-7}$	$-4.32215649 \times 10^{-11}$	$2.69556664 \times 10^{-15}$	0.05
H_2O	1.26011341×10^3	$2.87730230 \times 10^{-1}$	$5.30531503 \times 10^{-4}$	$-3.00478211 \times 10^{-7}$	$6.02885880 \times 10^{-11}$	$-4.24203019 \times 10^{-15}$	0.00
SO_2	2.97225003×10^2	$8.43288848 \times 10^{-1}$	$-5.92295509 \times 10^{-4}$	$2.05336002 \times 10^{-7}$	$-3.42687797 \times 10^{-11}$	$2.19991607 \times 10^{-15}$	0.00
Dry air	6.24216681×10^2	$2.79923458 \times 10^{-1}$	$-4.23992976 \times 10^{-5}$	$-1.59911855 \times 10^{-8}$	$6.00439662 \times 10^{-12}$	$-5.34217848 \times 10^{-15}$	

C_P	b_0	b_1	b_2	b_3	b_4	b_5	
N_2	9.61882185×10^2	$1.95531858 \times 10^{-1}$	$5.28590534 \times 10^{-5}$	$-5.87732131 \times 10^{-8}$	$1.42753440 \times 10^{-11}$	$-1.11597603 \times 10^{-15}$	75.53
O_2	7.68526781×10^2	$5.68661040 \times 10^{-1}$	$-3.53970739 \times 10^{-4}$	$1.22148573 \times 10^{-7}$	$-2.05538458 \times 10^{-11}$	$1.32813770 \times 10^{-15}$	23.14
Ar	5.19650000×10^2	0.00000000×10^0	0.00000000×10^0	0.00000000×10^0	0.00000000×10^0	0.00000000×10^0	1.28
CO_2	5.34680030×10^2	1.30016198×10^0	$-8.29823310 \times 10^{-4}$	$2.70087323 \times 10^{-7}$	$-4.32215649 \times 10^{-11}$	$2.69556664 \times 10^{-15}$	0.05
H_2O	1.72161341×10^3	$2.87730230 \times 10^{-1}$	$5.30531503 \times 10^{-4}$	$-3.00478211 \times 10^{-7}$	$6.02885880 \times 10^{-11}$	$-4.24203019 \times 10^{-15}$	0.00
SO_2	4.27025003×10^2	$8.43288848 \times 10^{-1}$	$-5.92295509 \times 10^{-4}$	$2.05336002 \times 10^{-7}$	$-3.42687797 \times 10^{-11}$	$2.19991607 \times 10^{-15}$	0.00
Dry air	9.04614051×10^2	$2.79923458 \times 10^{-1}$	$-4.23992976 \times 10^{-5}$	$-1.59911844 \times 10^{-8}$	$6.00439662 \times 10^{-12}$	$-5.34217848 \times 10^{-16}$	

capacities. That is, for the isentropic compression process in the dual cycle the first law of thermodynamics can be written as the partial differential equation

$$-P \partial v = C_v \, \partial T. \tag{7}$$

Noting also that, the equation of state for a perfect gas is

$$P = \frac{RT}{v}, \tag{8}$$

Eqs. (2) and (8) can be substituted into Eq. (7) to give

$$\left(-\frac{R}{v}\right) \partial v = \left(a_0 \frac{1}{T} + a_1 + a_2 T + a_3 T^2 + \ldots + a_n T^n\right) \partial T. \tag{9}$$

Integrating Eq. (9) over the compression process between points 1 and 2, yields Eq. (10) which is solved iteratively to find temperature at the end of the compression process, T_2, given an initial temperature, T_1 and the compression ratio, v_1/v_2.

$$-R \ln \frac{v_2}{v_1} = a_0 \ln \frac{T_2}{T_1} + a_1(T_2 - T_1) + \frac{a_2}{2}\left(T_2^2 - T_1^2\right) + \ldots + \frac{a_n}{n}(T_2^n - T_1^n). \tag{10}$$

The total heat added per cycle is assumed to be one part at constant volume, q_{Cv}, and the remainder at constant pressure, q_{Cp}. The cycle temperatures, T_3 and T_4, were found by solving Eqs. (12) and (14) respectively.

$$\partial q_{Cv} = C_v \partial T \tag{11}$$

$$=> \quad q_{Cv} = a_0(T_3 - T_2) + \frac{a_1}{2}\left(T_3^2 - T_2^2\right) + \frac{a_2}{3}\left(T_3^3 - T_2^3\right) + \ldots + \frac{a_n}{n+1}\left(T_3^{n+1} - T_2^{n+1}\right). \tag{12}$$

$$\partial q_{Cp} = C_P \partial T \tag{13}$$

$$=> \quad q_{Cp} = b_0(T_4 - T_3) + \frac{b_1}{2}\left(T_4^2 - T_3^2\right) + \frac{b_2}{3}\left(T_4^3 - T_3^3\right) + \ldots + \frac{b_n}{n+1}\left(T_4^{n+1} - T_3^{n+1}\right). \tag{14}$$

The expansion process from points 4–5 was calculated similarly to the compression process to calculate T_5

$$-R \ln \frac{v_5}{v_4} = a_0 \ln \frac{T_5}{T_4} + a_1(T_5 - T_4) + \frac{a_2}{2}\left(T_5^2 - T_4^2\right) + \ldots + \frac{a_n}{n}(T_5^n - T_4^n). \tag{15}$$

and the heat rejected, q_{out}, was calculated from T_5 and T_1

$$q_{out} = a_0(T_5 - T_1) + \frac{a_1}{2}\left(T_5^2 - T_1^2\right) + \frac{a_2}{3}\left(T_5^3 - T_1^3\right) + \ldots + \frac{a_n}{n+1}\left(T_5^{n+1} - T_1^{n+1}\right). \tag{16}$$

2.2. Evaluation of steady state cycle performance

While a variety of calculated cycle parameters are modified by the effects of the varying degrees of sophistication for the gas models discussed in Section 2.1, the calculated efficiency is relevant and useful for the purposes of illustrating these effects as this is a principal performance indicator for both the cycles and real engines. The results presented in Figs. 2.3 and 2.4 compare dual cycle efficiencies for; the standard, temperature-invariant, properties of air; the temperature-dependent properties of dry air from a linear to a fifth order polynomial relationship; the temperature-dependent properties of the cylinder gasses that account for gas composition, based on a sulphur-free fuel with a LCV = 43 MJ/kg, and mass composition of 86% carbon and 14% hydrogen, e.g. Diesel fuel. For ease of comparison, for the example presented in Fig. 2.3, cycle peak pressure has been fixed, and the compression ratio is varied with heat addition to achieve this and reflected in the heat addition ratio, defined as the proportion of the total heat added at constant volume to that added at constant pressure. The results selected for presentation includes compression ratios typical of real marine Diesel engines. In Fig. 2.4 the specific heat input is varied in the range 500–2800 kJ/kg, with the heat addition ratio set at 0.5. These specific heat input values are analogous to a lightly loaded engine up to an approximately stoichiometric AFR for the assumed fuel. Lines or *contours* connecting the same compression ratios and maximum temperatures, T_{MAX}, between each data set in the respective figures are provided for guidance.

Calculation Constants : Heat input, q_{in} = 1000 kJ/kg,
P_{MAX} = 100 bar, T_1 = 20 °C, P_1 = 1 bar

Calculation Constants : T_1 = 20 °C, P_1 = 1 bar,
Compression ratio = 20, Heat addition ratio = 0.5

In all cases, the increased sophistication of the gas models has the effect of reducing the calculated cycle efficiencies for otherwise the same nominal cycle conditions with greater reductions evident for
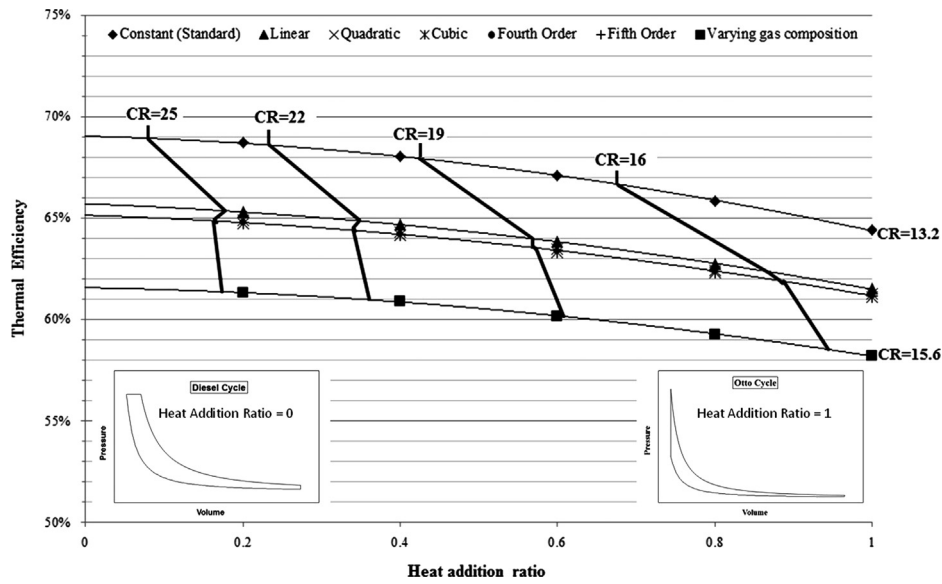
Fig. 2.3. Thermal efficiency of dual cycles over a range of heat addition ratios for different specific heat capacity models.
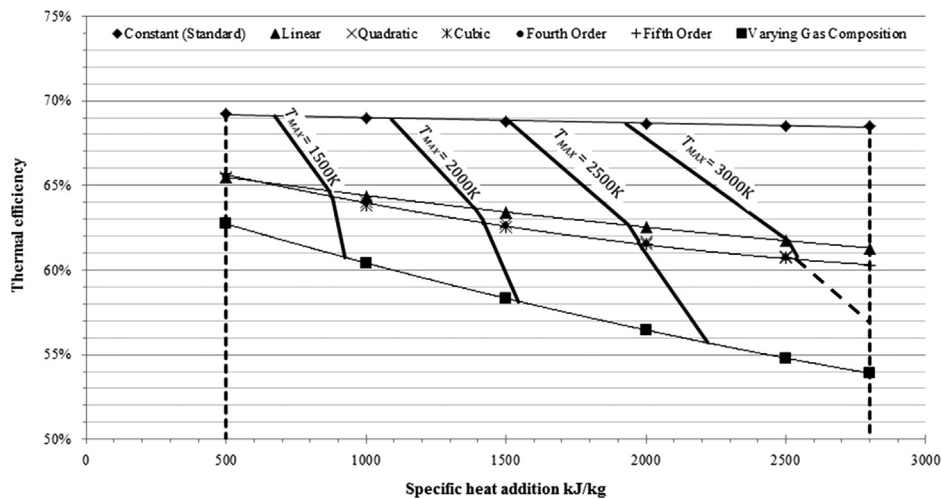

Fig. 2.4. Thermal efficiency of dual cycles over a range of specific heat addition values for different specific heat capacity models.

higher specific heat input. The implication being that increased sophistication in gas properties modelling are moving the calculated cycle efficiencies closer to those expected of a real engine. Accounting for temperature-dependent specific heat capacities, assuming dry air throughout the cycle, causes reductions of between four and eight per cent and additionally accounting for a change in gas composition causes further reductions by similar proportions. There are two reasons for the increase in the difference between the results at higher specific heat input values. Firstly, the specific heat capacities used in the temperature-dependent models become progressively higher than the standard values as the heat addition, and hence cycle temperatures, increase. The consequence is, as illustrated by the peak temperature contours in Fig. 2.4, the peak temperatures for the temperature-dependent models are progressively reduced as heat input increases, causing the observed increase in efficiency reduction between the standard dual cycle results and those using temperature-dependent specific heat capacities. Secondly, as the heat input increases, so does the assumed fuel mass and hence the assumed change in gas composition, causing the observed increase in efficiency reduction between the cycles using assumed dry air and those using the assumed change in gas composition.

Apparently, increasing the level of precision of the gas properties formulae has little effect on the calculated results for cycle thermal

efficiency beyond a quadratic representation and the claim of Al-Sarkhi et al. (2006) that the specific heat capacity variation can be represented as a linear function of temperature might be justified here. However, as illustrated in Fig. 2.2, the linear representation will overestimate the specific heat capacities in the lower temperature range and underestimate them in the higher temperature range. Therefore, for more sophisticated models in which accurate gas temperatures at all stages in the cycle are required, e.g. for predicting emissions formation, a prudent approach is to use a higher order representation as this adds little computational effort for the assured calculation precision.

This evaluation demonstrates the importance of including temperature-dependent and gas-composition sensitive specific heat capacity models in engine cycle model performance and these models, using fifth-order representations of gas properties, are therefore used in the more sophisticated time-based simulation models explained in Sections 3 and 4.

3. Time-based simulation

The motivations for adopting a time-based simulation approach for estimating engine performance are explained in

detail in Murphy and Pazouki (2012). Briefly put, the principal challenges of interest here for marine exhaust gas emission prediction, as outlined in Section 1.1, require that the prediction of performance over the full range of engine operational conditions is possible. In particular, this includes the, more challenging, time-dependent changing performance conditions when the coupled systems of engine-propeller-hulls are operated in transient conditions i.e. accelerating and decelerating, during e.g. manoeuvring operations in ports, in the vicinity of high population density, where the future focus of the emission prediction research lies. Furthermore, since the formation of NO$_x$, the prediction of which is of paramount interest from marine Diesel engines, is highly dependent on the time history of the exhaust gas conditions, further justifies a time-based approach to predicting these conditions. As also noted in (Murphy and Pazouki, 2012) the time-based simulation approach, while offering the advantages of being able to model transient conditions and exhaust gas time-history, has little draw-back for also modelling steady-state conditions, since the initial conditions of the integrators (see Fig. 3.1) within the simulation can be pre-set to accelerate the passage of (simulation) time towards a desired steady-state condition.

3.1. Description of the simulation methodology

As illustrated in Fig. 3.1, the simulation comprises a dynamic model of the engine system coupled with a thermodynamic model in the cylinder space. These models are simultaneously solved on a time-stepping basis to calculate the required derived outputs at any moment in (simulation) time, for both two-stroke and four-stroke engines. The dynamic and thermodynamic models are explained in the following sections with reference to Fig. 3.1.

3.1.1. The dynamic model

The dynamic model assumes a lumped-mass model of the engine and propulsion chain, similar to that assumed in dynamic response models for engine vibration and torsional responses. In this case a piston and crank model, as illustrated in Fig. 3.2, are coupled through their kinematic relationships, for displacement, velocity and acceleration.

For the piston, the net lateral forces are assumed to be zero, that is, the piston is constrained to travel in pure translation, up and down, within the cylinder, defined here as the x-direction. The resulting equation of motion for a single piston, using the reference system in Fig. 3.2 is

$$m_p \ddot{x} = F_c \cos \phi - F_p - m_p g \tag{17}$$

in which

$$F_p = \Delta PA \tag{18}$$

The crank and shaft elements are modelled as lumped-masses, constrained to move in pure rotation and while this neglects the detail of the connecting rod moving in general plane motion, an equivalent contribution to the total mass moment of inertia of the shaft can be included. The equation of the motion of the shaft is therefore

$$J_s \ddot{\theta} = -H_d F_c - T_p \tag{19}$$

The complete crank-piston system equation of motion then results through combining Eqs. (17)–(19) through the common connecting rod force

$$J_s \ddot{\theta} = -\frac{H_d m_p \ddot{x}}{\cos \phi} - \frac{H_d \Delta PA}{\cos \phi} - \frac{H_d m_p g}{\cos \phi} - T_p. \tag{20}$$

To solve this equation of motion, the dependency of piston linear acceleration, connecting rod angle and perpendicular distance, H_d, on shaft position, angular velocity and acceleration are also included, i.e.,

$$\sin \phi = \frac{r}{\ell} \sin \theta, \tag{21}$$

$$H_d = r \sin (\theta - \phi), \tag{22}$$

and

$$\ddot{x} = \ddot{\theta} \left[r \sin \theta - \frac{r^2 \sin \theta \cos \theta}{(\ell^2 - r^2 \sin^2 \theta)^{0.5}} \right] - \dot{\theta}^2$$
$$\times \left[\frac{r^2 (\cos^2 \theta - \sin^2 \theta)}{(\ell^2 - r^2 \sin^2 \theta)^{0.5}} + \frac{r^4 \sin^2 \theta \cos^2 \theta}{(\ell^2 - r^2 \sin^2 \theta)^{1.5}} - r \cos \theta \right] \tag{23}$$

Substituting Eqs. (23) into(20), the instantaneous angular acceleration of the shaft can be calculated from

$$\ddot{\theta} = -\frac{H_d m_p}{J_s \cos \phi} \left\{ \dot{\theta} \left[r \sin \theta - \frac{r^2 \sin \theta \cos \theta}{\left(\ell^2 - r^2 \sin^2 \theta \right)^{0.5}} \right] - \dot{\theta}^2 \right.$$
$$\left. \times \left[\frac{r^2 \left(\cos^2 \theta - \sin^2 \theta \right)}{\left(\ell^2 - r^2 \sin^2 \theta \right)^{0.5}} + \frac{r^4 \sin^2 \theta \cos^2 \theta}{\left(\ell^2 - r^2 \sin^2 \theta \right)^{1.5}} - r \cos \theta \right] \right\}$$
$$- \frac{H_d m_p g}{J_s \cos \phi} - \frac{H_d \Delta PA}{J_s \cos \phi} - \frac{T_p}{J_s} \tag{24}$$

Rearranging Eq. (24) gives

$$\ddot{\theta} \left\{ 1 + \frac{H_d m_p}{J_s \cos \phi} \left[r \sin \theta - \frac{r^2 \sin \theta \cos \theta}{\left(\ell^2 - r^2 \sin^2 \theta \right)^{0.5}} \right] \right\}$$
$$= + \frac{H_d m_p}{J_s \cos \phi} \dot{\theta}^2 \left[\frac{r^2 \left(\cos^2 \theta - \sin^2 \theta \right)}{\left(\ell^2 - r^2 \sin^2 \theta \right)^{0.5}} + \frac{r^4 \sin^2 \theta \cos^2 \theta}{\left(\ell^2 - r^2 \sin^2 \theta \right)^{1.5}} \right.$$
$$\left. - r \cos \theta \right] - \frac{H_d m_p g}{J_s \cos \phi} - \frac{H_d \Delta PA}{J_s \cos \phi} - \frac{T_p}{J_s} \tag{25}$$

For a multiple piston engine, under the assumption that each cylinder has the same physical characteristics and the effects of torsional vibration are neglected, Eq. (25) can be generalised to include any number, N, of pistons, i.e.,

$$\ddot{\theta} \left\{ 1 + \frac{m_p r}{J_s} \sum_{i=1}^{N} \frac{H_{di}}{\cos \phi_i} \left[\sin \theta_i - \frac{\sin \theta_i \cos \theta_i}{\left(\left(\frac{\ell}{r} \right)^2 - \sin^2 \theta_i \right)^{0.5}} \right] \right\}$$
$$= -\frac{m_p r}{J_s} \dot{\theta}^2 \sum_{i=1}^{N} \frac{H_{di}}{\cos \phi_i} \left[\cos \theta_i - \frac{\left(\cos^2 \theta_i - \sin^2 \theta_i \right)}{\left(\left(\frac{\ell}{r} \right)^2 - \sin^2 \theta_i \right)^{0.5}} \right.$$
$$\left. - \frac{\sin^2 \theta_i \cos^2 \theta_i}{\left(\left(\frac{\ell}{r} \right)^2 - \sin^2 \theta_i \right)^{1.5}} \right] - \frac{m_p g}{J_s} \sum_{i=1}^{N} \frac{H_{di}}{\cos \phi_i} - \frac{A}{J_s} \sum_{i=1}^{N} \frac{H_{di} \Delta P_i}{\cos \phi_i} - \frac{T_p}{J_s} \tag{26}$$

Eq. (26) is the "Dynamic Governing Equation" in Fig. 3.1 which is used to calculate the angular acceleration of the shaft at each time step. This is then integrated once to give instantaneous shaft rotational velocity and again to give instantaneous shaft angle. These are then used to back-calculate instantaneous specific volumes and volume time derivatives required in the thermodynamic model. While not a necessary limitation of the model, in the studies reported here, the shaft rotational velocity is also used as the simulated control signal for the system so that heat addition, per-power-stroke, is adjusted through a PID control algorithm as the engine speed governor.

The inputs to the dynamic model come from; specification of the physical engine characteristics required for solving Eq. (26), the instantaneous gas pressure differential, ΔP, which comes from the thermodynamic model, the frictional and load torque models; summed to give total shaft torque, T_p. There are a number of friction

Fig. 3.1. Schematic of the time-based simulation solver methodology indicating the principal interactions between the incorporated sub-models.

Fig. 3.2. Definition sketch of a piston-con rod-crank arrangement.

models for reciprocating engines, e.g. as a function of piston speed and stroke (Angulo-Brown et al. 1993) and the use of the Willan's line method (e.g. Heywood, 1988). The latter is used in the studies in this

paper as explained in Section 4. The load torque model can simply be specified to suit the actual characteristics of the attached load, e.g. for a ship, the propulsor performance curves. In this paper the load

torque characteristics match those of the dynamometer attached engine used in the physical experiments reported in Section 4.

3.1.2. The thermodynamic model

For the time-dependent thermodynamic model the time derivative of the first law of thermodynamics is used for the trapped gases in the cylinders, i.e.

$$\frac{dq}{dt} - \frac{dw}{dt} = \frac{du}{dt}. \tag{27}$$

since

$$du = C_v dT, \tag{28}$$

$$dw = P dv \tag{29}$$

and

$$P = \frac{RT}{v}, \tag{30}$$

Making the appropriate substitutions, Eq. (27) can be expanded to

$$\frac{dq}{dt} - \frac{dv}{dt}\left(\frac{RT}{v}\right) = \frac{dT}{dt}(C_v). \tag{31}$$

noting that

$$\frac{R}{C_v} = \gamma - 1 \tag{32}$$

and using the dot notation for time derivatives, Eq. (28) can be rewritten as

$$\dot{q} - \dot{v}\left(\frac{T}{v}\right)(\gamma - 1) = \dot{T}. \tag{33}$$

Eq. (33) is the "Thermodynamic Governing Equation" in Fig. 3.1, used to calculate the time derivative of gas temperature, which is then integrated to give cylinder gas temperature at each time step.

As illustrated in Fig. 3.1, aside from those of the dynamic model, already discussed, the inputs to the thermodynamic model come from; the gas properties model, the heat addition model and the heat loss model; these last two summed to give, $\dot{q}$. In the code there are a variety of user-specified choices for heat input and gas composition models, including the option to specify invariant gas properties throughout the simulation as demonstrated in Section 4.1. Nevertheless, based on the outcomes of the studies presented in Section 2, the heat input and gas properties models can also be specified to jointly follow the most sophisticated principles detailed in that section,

i.e. accounting for temperature-dependent and gas-composition-dependent properties of the cylinder gases, which can also in- or ex-clude residual exhaust gasses remaining in the cylinder from the preceding cycle. In addition, there are a variety of time-dependent heat-rate addition models available to the user to permit future research of the sensitivities of the simulation results on the underlying assumptions therein. That used in the studies presented in Section 4, generally accepted as an accurate estimate, are in close approximation to the Wiebe function (Wiebe, 1956) as exemplified in the insert to achieved solutions closer to that of the actual Otto cycle as demonstrated in Fig. 4.4.

Heat loss can be calculated by assuming convective heat transfer from the cylinder gasses to the cylinder walls where the cylinder walls are assumed to have constant temperature and the heat transfer coefficient is calculated by an empirical formula such as the well-known Woschni correlation (Heywood, 1988; Woschni, 1967). While a variety of options are available in the code, a similar, 1D approach is adopted in the studies reported in this paper and, based on the accuracy of the results in Section 4, this indicates the robustness of this approach, in particular, in view of the stated aim to permit reasonably accurate engine performance, given sparse input data across a wide variety of engine types and operating conditions.

4. Selected results from the time-based simulation

To verify the accuracy of the simulation, extensive numerical, theoretical and experimental trials have been conducted. In this paper a selection of the key results are presented. These are as follows:

- A comparison between the air-standard Otto cycle and a simulation of the same using MESS (Section 4.1).
- Results from MESS on the inclusion of varying gas properties and composition, analogous to the dual cycle studies of Section 2 (Section 4.2).
- Results from the progressive inclusion of the thermodynamic sub-models from Fig. 3.1 and the inclusion of modelling cylinder residual exhaust gas (Section 4.3).
- Results demonstrating the ability of MESS to accurately predict the performance of a real Diesel engine, operating across a range of steady state conditions (Section 4.4).
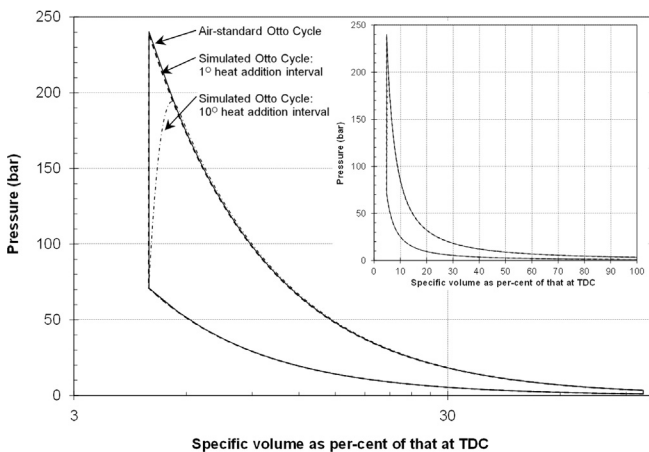

Fig. 4.1. P–v diagrams of an air-standard Otto cycle compared to approximations of an Otto cycle performed by simulation. All cycles have a specific heat input of 1695 kJ/kg and compression ratio is 21. The inset uses linear scales whereas the main figure uses a logarithmic volume axis to highlight the otherwise almost imperceptible differences in the low volume region.
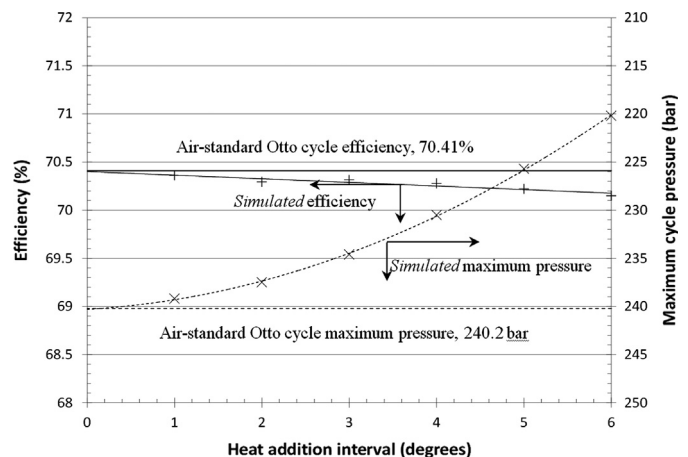

Fig. 4.2. Simulated cycle efficiencies and maximum pressures as a function of heat addition interval.
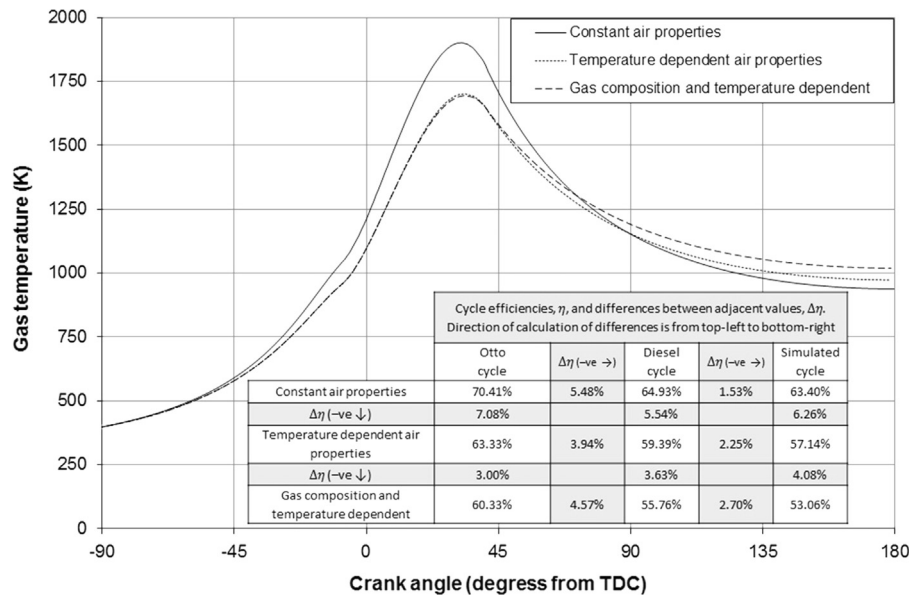
Fig. 4.3. Simulated Temperature–Crank angle diagram showing the effects over the cycle of varying gas properties and gas composition. Heat input is 1210 J kg^{-1} K^{-1} beginning at 10º BTDC and finishing at 40º ATDC and compression ratio is 21.
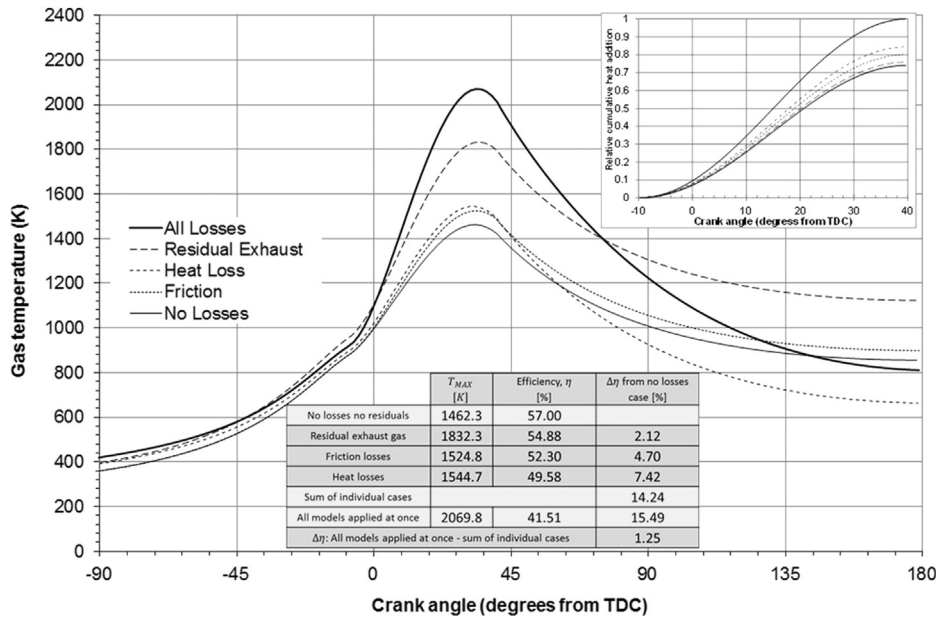

Fig. 4.4. Simulated Temperature–Crank angle diagram showing the effect of losses and residual exhaust gas inclusion. Comparison is on the basis of the engine running at the same speed with the same shaft torque in each case. The inset graph shows the non-dimensional cumulative heat addition required in each case.

4.1. A comparison with the air-standard Otto cycle

If the simulation is *numerically* accurate, it will, at least, produce the same results as an air-standard dual cycle, be it the Otto, dual or Diesel cycle, if the heat addition conditions in the time-based simulation can be controlled to be equivalent of those in the corresponding air-standard cycle. Of course, just as in a real engine, because the simulation is dynamic and time-based, it is not possible to contrive a heat addition function that will simulate heat addition under constant pressure conditions. On the other hand, a constant volume heat addition process, in the time-domain, is analogous to an instantaneous heat addition process and, while this is still not possible to achieve exactly in the time-based simulation, with appropriate selection of the simulation time-stepping intervals to ensure numerical convergence, the heat addition was specified to occur over progressively shorter crank intervals beginning at TDC, so

that the simulation progressively Figs. 4.1 and 4.2. All sub-models for losses and varying gas properties are disabled so standard air properties with zero losses are used throughout the simulations. As illustrated in Fig. 4.1, the differences between the simulated P–v diagrams with the heat addition interval set to 1º of crank angle (dashed line) and the air-standard Otto cycle (solid line) are almost imperceptible, even with the slightly unconventional use of a logarithmic volume scale, which has been purposefully used here to accentuate these differences, i.e. as per the inset to Fig. 4.1, showing the same data on linear scales. For comparison, the simulated cycle with a 10º (of crank angle) heat addition interval (dash-dot line) has also been included as a demonstration that differences do become apparent as the simulated cycle moves away from a close approximation to the Otto cycle. In Fig. 4.2, using both cycle efficiencies and maximum pressures, the convergence towards the actual Otto cycle values as the simulated heat addition interval is

reduced is self-evident and reveals the approach detailed in Section 3 is theoretically sound.

4.2. Effects on simulated results of varying gas properties and gas composition models

Fig. 4.3 provides an illustration of the effects on the simulated cycle of progressively increasing the sophistication of the gas properties model, similar to the studies in Section 2. For both cycles using temperature dependent specific heat capacities, the cycle temperatures are coincident up until end of compression, in this case, at 10° BTDC since to that point no fuel/heat addition has occurred, and in both cases, as expected the cycle temperatures are below those of the model assuming the net lower constant air-standard specific heat capacity. As fuel combustion/heat addition progressively occurs between 10° BTDC and 40° ATDC the gas temperatures calculated from the gas composition model can be observed to depart from those calculated with the temperature dependent-only model. This re-emphasises the importance of including the more sophisticated gas properties models in a time-based simulation that needs to reliably predict gas temperature time histories across the complete cycle.

As a means of making back-reference to the benchmarking studies using the dual cycle in Section 2, the total cycle efficiencies simulated using each model are also compared in the inserted table to Fig. 4.3 to those calculated using the Otto and Diesel cycles (essentially the two extremes of the heat addition ratio specification for the dual cycle) with the same initial cycle conditions, heat addition and gas properties models.

Looking across the table from left to right, as might be expected, regardless of the gas properties model employed, in each case, the effect of "rounding the corners" in the simulated machine cycles as compared to the "straight-edged" constant volume-pressure combinations in the Otto-dual-Diesel cycles can be observed here to reduce the efficiency below that included between the extremes of the dual cycle for the same nominal cycle conditions, with the $\Delta\eta$ values indicating a consistency of behaviour. However, although this exercise is neglecting external losses (e.g. friction and cooling), as included in the proceeding sections, as an academic observation, it is interesting to note that there is some similarity between the thermodynamic efficiency predicted by the simulated machine cycle and the Diesel cycle which might prove useful information for future studies.

Looking down the table from top to bottom, there is again a notable consistency of behaviour as the increasingly sophisticated gas properties models are applied to the purely theoretical Otto-dual-Diesel cycles as well as the simulated cycles, thus indicating that the trends, and subsequent recommendations, noted in the studies of Section 2 are equally valid for the simulated machine cycles.

4.3. The effect on the simulated results of modelling losses and accounting for residual exhaust gases

As indicated in Fig. 3.1 to simulate actual engine operation, losses are also considered, namely heat loss through the cylinder walls and friction losses. Furthermore, having noted the effect of gas composition on the analytical and simulated results an estimate of the residual exhaust gases left in the cylinder at the start of each cycle can be included. Fig. 4.4 provides an example of the effects of each of these additional considerations on the simulated results as each one is applied individually together with the net effect when they are all applied simultaneously. In each case the simulation is run, the control system heat addition is allowed to vary automatically to maintain a constant simulated shaft speed of 1500 RPM (a value consistent with the engine speeds considered in the physical experiments reported in Section 4.4).

Table 4.1
Specifications of the engine used for the experimental data.

Cycle	4-Stroke
Nominal Rated (max.) Power	3.5 kW
Speed range	1200–3600 RPM
Other characteristics	Air cooled, direct injection, naturally aspirated
Compression ratio	21:1
Cylinders	1
Bore	69 mm
Stroke	60 mm
Cylinder volume	225 cm^3

Modelling the inclusion of each loss has a unique effect. Heat transfer to the cylinder walls causes an increase to the cylinder temperature during compression and therefore increases peak temperature but the net result is a loss of heat energy. Friction draws more heat input to reach the same shaft speed. All three effects individually reduce the efficiency and, when combined, result in efficiency values which are possible with actual cycles. By calibrating the inputs to model experimental data it is possible to accurately produce outputs of efficiency and work as demonstrated in Section 4.4.

4.4. Experimental validation of the Marine Engine System Simulation

For the purposes of this paper, experimentation has been carried out on a Diesel engine with the specifications listed in Table 4.1.

Having already demonstrated the ability of the simulation to provide good agreement with power-card diagrams in earlier work (Murphy and Pazouki, 2012), here the focus was to demonstrate the more challenging task of simulating accurate engine performance over a wide power band of the engine operating conditions. Figs. 4.5 and 4.6 illustrate a selection of engine test data compared with the results simulated with MESS. In these figures, each adjacent pairs of data (in some cases overlapping) indicate the experimental and simulated result under the same nominal conditions. Clearly, the incorporation of losses, a more advanced heat addition model and the time-based calculation has produced accuracy which could not be simulated by ideal models and indeed in all cases the simulated results are in remarkable agreement with the test data. Essentially, Fig. 4.5 indicates that the mechanical simulation models are robust, in particular the modelling of frictional losses, with the close agreement of the shaft torque data along the Willan's lines. In addition, by implication, Fig. 4.5 also shows that the accuracy of the predicted efficiency is in close agreement in each case because the same specific heat input produces the same engine torque and speed. Fig. 4.6 provides a proxy for indicating the accuracy of the thermodynamic models, including incorporation of aforementioned gas properties models and heat loss models. That is, it is particularly challenging to get cycle temperatures (for which the exhaust gas temperature, in this case, is used as an indicator for) and engine power values to be simultaneously calculated in agreement with actual engine data, which is the case as indicated in Fig. 4.6. Furthermore, and of critical importance, the data is in agreement across a broad range of engine operational conditions, in this case, in the range approximately 14–63% MCR.

5. Conclusions

In the context of resolving the dilemma between the need for accurate coupled mechanical-thermodynamic models required for predicting marine engine performance, and in particular, the time-varying thermodynamic gas properties to feed complex emissions
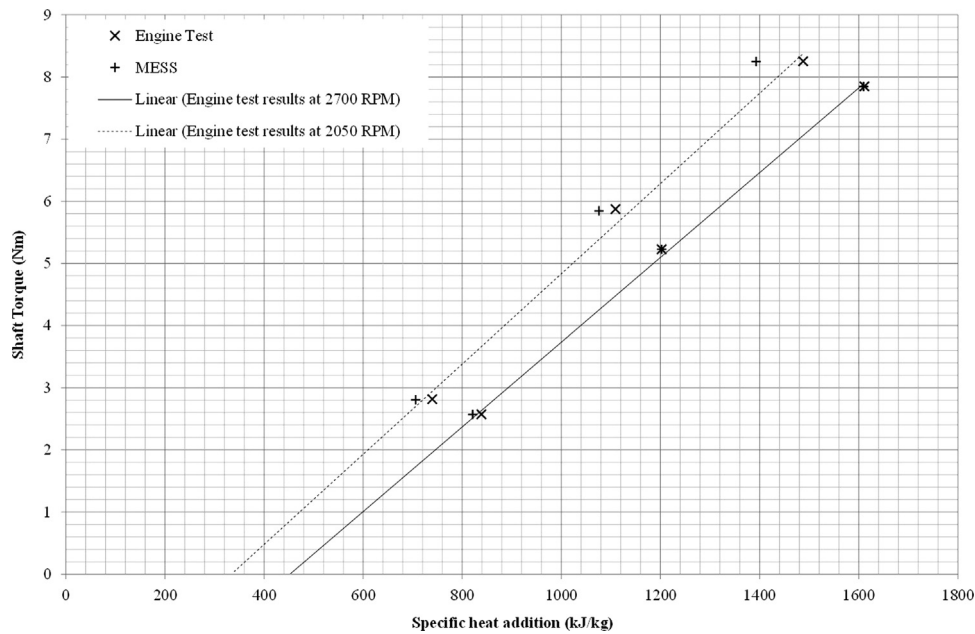
Fig. 4.5. Engine test data plotted with simulated data of shaft torque and heat addition. The Willan's lines are plotted for engine test data only.
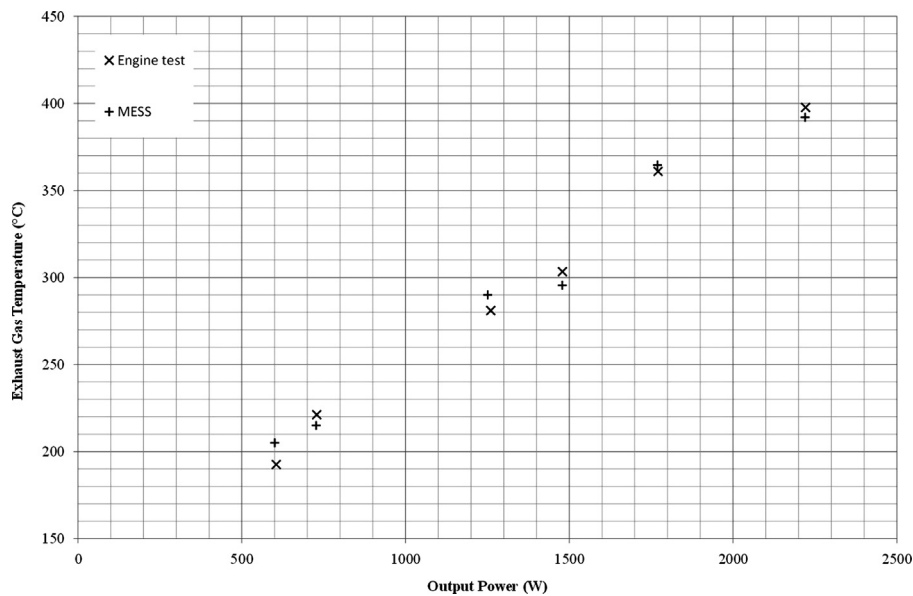

Fig. 4.6. Engine test data plotted with simulated data of exhaust temperature and output power.

calculations, yet with sparse and varied input data, the significance of the levels of sophistication of modelling gas properties, gas composition has been examined. This work has shown that, although simplified gas property and composition models can inform qualitative analyses and provide gross estimates of e.g. overall thermal efficiency, the precise simulated time-history of the thermodynamic properties in the cylinder space, essential for emission modelling, are critically dependent on using an accurate and sophisticated model.

Taking this conclusion, a time-domain engine simulation has been developed, which is capable of modelling two or four stroke cycles in steady-state or transient operation. A comparison with the air-standard Otto cycle has validated the numerical accuracy of the simulation and the success of this approach has been demonstrated through simulations of actual engine performance which

shows remarkably close and consistent correlation over a wide range of engine operating conditions.

Having demonstrated the validity of this approach for modelling engine performance further studies are now required to couple the time-varying outputs of cylinder space conditions to refined emission models.

Acknowledgements

References

Al-Sarkhi, A., Jaber, J.O., Abu-Qudais, M., Probert, S.D., 2006. Effects of friction and temperature-dependent specific-heat of the working fluid on the performance of a Diesel-engine. Appl. Energy 83, 153–165.

Angulo-Brown, F., Fernandez-Betanzos, J., Diaz-Pico, C.A., 1993. Compression ratio of an optimized air standard Otto-cycle model. Eur. . Phys. 15, 38–42.

Baulch, D.L., Cobos, C.J., Cox, A.M., Frank, P., Haymann, G., Just, T., Kerr, J.A., Murrels, T., Pilling, M.J., Twe, J., Walker, R.W., Warnatz, J., 1991. Compilation of rate data for combustion modelling. J. Phys. Chem. Ref. Data 22, S847.

Buhaug, Ø., Corbett, J.J., Endresen, Ø., Eyring, V., Faber, J., Hanayama, S., Lee, D.S., Lee, D., Lindstad, H., Markowska, A.Z., Mjelde, A., Nelissen, D., Nilsen, J., Pålsson, C., Winebrake, J.J., Wu, W., Yoshida, K., 2009. Second IMO GHG Study. International Maritime Organization (IMO), London, UK.

Chase, M.W., Davies, C.A., Downey, J.R., Frurip, D.J., McDonald, R.A., Syverud, A.N., 1986. JANAF Thermochemical Tables, American Chemical Society, 3rd Ed. American Institute of Physics for the National Bureau of Standards, Washington, DC, USA.

Chesse, P., Chalet, D., Tauzia, X., Hetet, J.F., Inozu, B., 2004. Real-time performance simulation of marine Diesel engines for the training of Navy crews. Mar. Technol. 41, 95–101.

Eastop, T.D., McConkey, A., 1993. Applied Thermodynamics for Engineering Technologists, 5th Ed. Longman Scientific and Technical, Essex, UK.

Ferguson, C.R., 1986. Internal Combustion Engines, Applied Thermosciences. John Wiley & Sons, Inc., New York, USA.

Jackson, L., Russell, P.A., Morton, T.D., 2012. Reeds Vol 12 Motor Engineering Knowledge for Marine Engineers. Bloomsbury Publishing, London, UK.

Merker, P.G., Schwarz, C., Stiesch, G., Otto, F., 2005. Simulating Combustion. Springer, New York, USA.

Heywood, J.B., 1988. Internal Combustion Engine Fundamentals. McGraw-Hill, Inc., New York, USA.

Hountalas, D.T., 2000. Prediction of marine Diesel engine performance under fault conditions. Appl. Therm. Eng. 20, 1753–1783.

Keenan, J.H., Chao, J., Kaye, J., 1983. Gas Tables: International Version: Thermodynamic Properties of Air Products of Combustion and Component Gases Compressible Flow Functions, 2nd Ed. John Wiley & Sons, Inc., New York, USA.

Kilpinen, P., 2010. Optimization of a simplified sub-model for NO emission prediction by CFD in large 4-stroke marine Diesel engines. Fuel Process. Technol. 91, 218–228.

Lloyd's Register of Shipping, 1995. Marine Exhaust Emissions Research Programme. Lloyd's Register of Shipping, London, UK.

Murphy, A.J., Pazouki, K., 2012. Exhaust Gas Emissions from Regional Shipping: Mitigating Technologies and Emission Prediction. International conference on The Environmentally Friendly Ship. The Royal Institution of Naval Architects, London.

Payri, F., Olmeda, P., Martín, J., García, A., 2011. A complete 0D thermodynamic predictive model for direct injection Diesel engines. Appl. Energy 88, 4632–4641.

UNCTAD, 2013. United Nations Conference on Trade and Development, Review of Maritime Transport 2013. ISBN 978-92-1-112872-7.

Woodyard, D., 2009. Pounder's Marine Diesel Engines and Gas Turbines, 9th Ed. Elsevier Butterworth-Heinemann, London, UK.

Wiebe, I.I., 1956. Semi-empirical expression for combustion rate in engines, In: Proceedings of the Conference on Piston engines, Academy of Sciences, Moscow, USSR pp. 185–191.

Woschni, G., 1967. A Universally Applicable Equation for the Instantaneous Heat Transfer Coefficient in the Internal Combustion Engine. SAE Technical Paper.

Write, A.A., 2000. exhaust emissions from combustion machinery. Marine Engineering Practice Series, vol. 3. The Institute of Marine Engineers, London, UK.

Zeldovich, Y.B., 1946. The oxidation of nitrogen in combustion and explosions. Acta Physiochim. 21, 577–628.